Mechanically-Sensitive Fluorochromism by Molecular Domino Transformation in a Schiff Base Crystal

Toshiyuki Sasaki,[a*]† Takanori Nakane,[b] Akihiro Kawamoto,[b] Yakai Zhao,[c,d] Yushi Fujimoto,[e] Tomohiro Nishizawa,[f] Fuyuki Ito,[e*] Upadrasta Ramamurty,[c,d*] Ranjit Thakuria,[g*] Genji Kurisu[b,h,i*]

[a]Graduate School of Nanobioscience, Yokohama City University, 22-2 Seto, Kanazawa-ku, Yokohama, Kanagawa 236-0027, Japan. E-mail: tsasaki@yokohama-cu.ac.jp

[b]Institute for Protein Research, Osaka University, 3-2 Yamadaoka, Suita, Osaka 565-0871, Japan.

[c]School of Mechanical and Aerospace Engineering, Nanyang Technological University, Singapore 639798, Singapore. Email: satwiku@gmail.com

[d]Institute of Materials Research and Engineering, Agency for Science, Technology and Research (A*STAR), Singapore 138634, Singapore.

[e]Department of Chemistry, Institute of Education, Shinshu University, 6-ro, Nishinagano, Nagano, 380-8544, Japan. Email: fito@shinshu-u.ac.jp

[f]Graduate School of Medical Life Science, Yokohama City University, 1-7-29 Suehiro-cho, Tsurumi-ku, Yokohama 230-0045, Japan.

[g]Department of Chemistry, Gauhati University, Guwahati 781014, Assam, India. Email: ranjit.thakuria@gmail.com, ranjit.thakuria@gauhati.ac.in

[h]JEOL YOKOGUSHI Research Alliance Laboratories, Graduate School of Frontier Biosciences, Osaka University, 1-3 Yamadaoka, Suita, Osaka 565-0871 Japan.

[i]Institute for Open and Transdisciplinary Research Initiatives, Osaka University, 2-1 Yamadaoka, Suita, Osaka 565-0871, Japan. Email: gkurisu@protein.osaka-u.ac.jp

ABSTRACT: The ability to make large changes in properties against small external stimuli is one of key factors in sensing materials. Molecular domino transformation, i.e. polymorphic transformation starting at a stimulated point and extending to the whole crystal, is an attractive phenomenon from this viewpoint. We recently found such a transformation in a crystal of 4-nitro-N-salicylideneaniline as one of Schiff bases. In this study, quantitative evaluations were conducted on a mechanical stimulus and emission properties in the transformation of the crystal. Our results demonstrate the potential applicability of the crystal to detection of even less than a few µN mechanical stimuli as an emission color change. A molecular level transformation mechanism revealed by microcrystal electron diffraction also contributes to future development of the transformation-based materials.

Introduction

Molecular crystals can alter their properties in response to external stimuli by conversion of molecular structures, molecular arrangements, and/or crystal's components.[1–3] Various kinds of external stimuli, such as thermal,[4–9] mechanical,[10–15] light,[16–18] and vapor-based stimuli,[19–

[21] have been used to induce the conversion. Remarkable property changes and high sensitivity to external stimuli are reported; tailoring of such changes can lead to fascinating sensing and actuation applications.

Molecular domino transformation (MDT), discovered and named by Ito et al. in a gold(I) complex in 2013,[11] is one such possible mechanisms to achieve the desired characteristics. Not only is the transformation inducible by a small mechanical stimulus but it also progresses from the initial point through the entire crystal autocatalytically. Such domino-like amplification of the response to mechanical stimulus enables the molecular crystals to detect mechanical stimuli with high sensitivity. However, MDT is reported only in a small number of molecular crystals hitherto.[9,11,12] Therefore, research on it has depended mostly on serendipity. For further rational development of sensing materials that use MDT as the main mechanism, fundamental understanding of it and in a wider variety of molecular systems is necessary.

Salicylideneaniline derivatives have been selected as a model system for this purpose because of their remarkable polymorph-dependent fluorescence properties[22,23] as well as their easy availability via a condensation reaction of anilines and salicylaldehydes. Herein, we characterize MDT in a crystal of 4-nitro-*N*-salicylideneaniline (**1**). In addition to the evaluation of the emission characteristics by fluorescent microscopy, the mechanical sensitivity and the molecular level mechanism of the transformation are investigated using nanoindentation[24–27] and microcrystal electron diffraction (MicroED) techniques,[28–35] respectively.

Results and Discussion

Fluorescent properties. 1 was synthesized by a condensation reaction of 4-nitroaniline and salicylaldehyde in ethanol. Recrystallization of **1** from THF resulted in columnar orange crystals (Figure 1b). Two types of crystals were observed. Upon UV (365 nm) light irradiation, one type emits strong yellow color while the other emits weak orange color. Hereafter, these two crystal polymorphs are referred as **1Y** and **1O**, respectively (Figure 1c(i)). Such remarkable emission color differences between polymorphs are often observed in molecular crystals showing excited-state intra-proton transfer (ESIPT): an intra-proton transfer from an excited enol to an excited keto form causes an emission spectral redshift.[16,23,36–38] Their emission spectra were recorded by a fluorescent microscope (IX71, Olympus Co., Ltd.) with a spectrometer (USB4000, Ocean Optics Co., Ltd.) as shown in Figure 1c(ii). **1Y** has two emission peaks at 567 and 606 nm while that of **1O** is at 614 nm with a shoulder at 580 nm. A shorter fluorescence lifetime of **1O** than that of **1Y** indicates that non-radiative relaxation pathways have larger contribution to the fluorescence of **1O** than **1Y** (Figure S4) In addition, spatially resolved fluorescent measurements by a hyperspectral camera (SI-108, EBA JAPAN Co., Ltd.) revealed their non-uniform emission properties (Figure 1d). The relative intensity of emission peaks around 570 and 610 nm changes depending on measurement points in both crystals. Note that emission from the edge of **1Y** (region 3 in Figure d(i)) shows a spectrum resembling that of **1O** when compared to the middle region (region 2 in Figure d(i)). We surmise that the emission heterogeneity is due to the formation of a mixed crystal of **1Y** with a small portion of **1O**. The ratio of **1O** at the edge is larger than that at the middle. Such kind of intergrowth polymorphs have been investigated by Desiraju and coworkers on aspirin[39] and felodipin[25] molecular crystals.
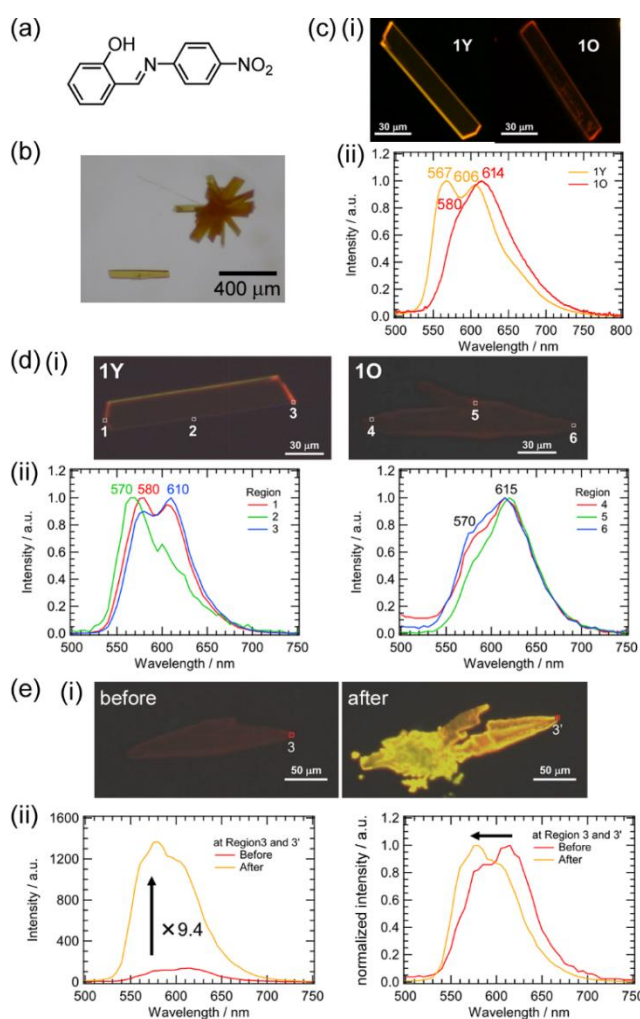
Figure 1 Fluorescent properties of 1Y and 1O. (a) Molecular structure of **1**. (b) Photographic images of **1** under white light. (c)–(e) (i) Photographic images of **1Y**, **1O**, **1O** before transformation (before), and after transformation (after) under UV light and (ii) their emission spectra. Emission spectra in (c) were recorded by a fluorescent microscope (IX71, Olympus Co., Ltd.) with a spectrometer (USB4000, Ocean Optics Co., Ltd.) while those in (d) and (e) were measured by a hyperspectral camera (SI-108, EBA JAPAN Co., Ltd.).

Interestingly, **1O** shows emission color change upon mechanical stimuli (Figure 1e). Orange emission from **1O** transformed into yellow at the stimulated area. The yellow emission area gradually spreads over the whole crystal, suggesting the operation of MDT in the crystal[11] that transforms it from **1O** to **1Y**. The transformation was also confirmed by spatially resolved emission spectra recorded by a hyperspectral camera. The emission spectrum obtained at the regions 3 of **1O** in Figure 1e has strong and relatively weak peaks at 610 and 580 nm, respectively. The relative intensities of the peaks become the opposite after the transformation and the resulting spectrum nearly-corresponds to that of as-prepared **1Y**. Moreover, the emission intensity increased by 9.4 times after the transformation.

Mechanical investigation of the phase transformation. Sensitivity of **1O** against mechanical stimuli was investigated using nanoindentation (Figure 2).[24–27] **1O** for nanoindentation studies was prepared by evaporation of the THF solution dropped on a glass plate under air at room temperature. More than 20 crystals of **1O** prepared on glass plates

were stimulated by a diamond indenter tip with maximum applied load ranging from 1 to 3,000 µN. The transformation of the stimulated crystals was confirmed by emission color change. The large variation in the force required for triggering the transformation could have origins in a variety of factors such as the crystal size, shape, local surface topology, how firmly the crystal is attached to the substrate, and so on. Some crystals showed high mechanical sensitivities, i.e. they underwent the transformation at forces as low as 1 µN.
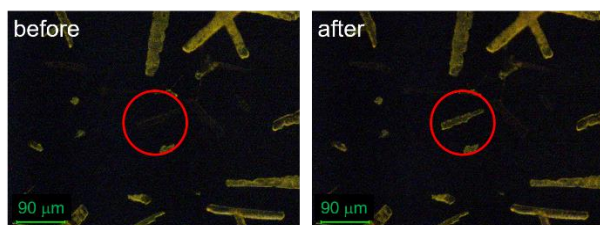

Figure 2 Photographic images of 1. 1 under UV light before and after nanoindentation (Hysitron TI980, Bruker Corp.). Mechanically stimulated **1O** is circled by red.

Crystallographic studies. The origins of the different emission properties and structural stabilities of **1O** and **1Y** were investigated based on their crystal structures. Due to **1O**'s mechanical sensitivity to transform into **1Y**, large single crystals of **1O** could not be mounted on a conventional X-ray diffractometer. Thus, crystal structures of **1O** and **1Y** were determined by microcrystal electron diffraction (MicroED) (Figures 3, 4).[28–35] For this purpose, microcrystalline **1O** and **1Y** were prepared directly on a copper EM grid (Quantifoil R1.2/1.3 Cu 200 mech) by 'painting' the THF solution, not crystal suspension, using a brush to prevent any possible mechanical stimulation of the crystals and loaded onto a Talos Arctica microscope (Thermo Fisher Scientific) equipped with a Ceta detector (CMOS 4k x 4k, Thermo Fisher Scientific). Data collection was performed using SerialEM[40] with a strategy described in the literature.[34,35,41,42] Diffraction patterns from more than 1150 crystals were measured at 200 kV with an electron flux of 0.05 $e^-Å^{-2}s^{-1}$. Diffraction patterns were indexed, integrated, and scaled using DIALS.[43–45] First, crystals were indexed without using any prior cell information and the Bravais lattice constraints. The distribution of resulting unit cell parameters indicated the presence of two crystal forms (monoclinic and orthorhombic) in the sample (Supporting information Fig. S2). Next, the dataset was reprocessed twice, using the cell parameter and lattice type of each crystal form. Crystals in each group were further clustered by xia2.multiplex[46] to find the best sets of crystals for final merging (Supporting information Tables S1, S2). 697 crystals were indexed in the monoclinic crystal form and 55 good crystals were merged. The structure was solved in the space group $P2_1/c$ and was identical to the **1Y** structure solved by X-ray diffraction in previous studies.[47,48] A powder X-ray diffraction pattern of **1Y** agrees well with that simulated from the solved structure (Supporting information Fig. S3). Other 90 crystals were indexed in the new orthorhombic crystal form and 4 best crystals gave a structure in the $Pna2_1$ space group. We assigned this to be **1O**. The crystal structures were solved using SHELXT[49] and refined kinematically by SHELXL[50] in Olex2 GUI (Supporting information Table S3).[51,52]

There are two crystallographically independent molecules of Z1 and Z2 in **1O**; the dihedral angles between the two phenyl groups in them are $\theta_d=36.2°$ and 35.1°, respectively (Fig. 3a(i)). Such large θ_d could be one of the origins of the low emission intensity due to twisted intramolecular charge transfer.[23,37,53–55] The π-π distance (d_π) between Z1 (or Z2) molecules is ca. 3.4 Å (Fig. 3a(ii)). In addition to the intramolecular hydrogen-bonding between hydroxyl and imino groups (N···O distance of $d_{N-O}=2.66$ Å), **1** forms an intermolecular hydrogen bond between the hydroxyl groups (O···O distance of $d_{O-O}=2.89$ Å) of Z1 and Z2 to afford a

hydrogen-bonded dimer (Fig. 3a(iii)). The dimer tilts ca. 29° against the *c* axis and stacks along the *b* axis with a distance of d_π=3.4 Å to form a columnar assembly (Fig. 3b). Two-fold helices in **1O** are perpendicular to the stacking direction.
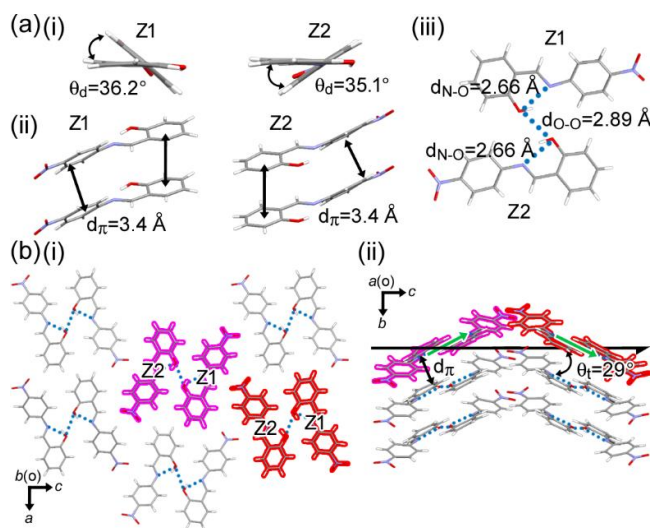
Figure 3 Crystallographic studies of 1O. (a) (i) Dihedral angle, θ_d, between the two phenyl rings, (ii) distances between π-stacked molecules, (iii) hydrogen-bonding dimer, (b) (i) packing diagram, and (ii) side view of a right-handed two-fold helix by neighboring columns in **1O**. The helical handedness is defined by tilt (green arrow) of the dimer according to the supramolecular-tilt-chirality method.[56–58]

In contrast to **1** in **1O**, **1** in **1Y** is almost planar, *i.e.,* the two phenyl groups are nearly parallel (θ_d=3.8°) (Fig. 4a(i)). This value is much smaller than that noted in **1O** (θ_d=36.2°, 35.1°). According to the literature, enol and keto forms are stable in a salicylideneaniline derivative with small (less than about 12°) and large θ_d, respectively.[23] Hence, the intense emission of the long wavelength than the short one in **1O** and the opposite trend in **1Y** are most likely due to these stability differences. In addition, the correlation between θ_d and fluorescence lifetimes corresponds with those reported in the literature. d_π between Z1 molecules is 3.0–3.5 Å (Fig. 3a(ii)). Similar to **1O**, **1** forms a hydrogen-bonding dimer with intra- and inter-molecular hydrogen-bonding N⋯O (d_{N-O}=2.66 Å) and O⋯O (d_{O-O}=3.00 Å), respectively (Fig. 4a(iii)). The dimer tilts ca. θ_t=25° against the *b* axis and stacks with an inversion symmetry at a distance of d_π=3.0–3.5 Å along the *b* axis to form a columnar assembly. Neighboring columns are related by a two-fold helical symmetry along the stacking direction in a herringbone manner (Fig. 4b). The π-stacking manner of **1** is parallel in **1O** while that in **1Y** is antiparallel. These packing differences could also be another reason for the observed differences in the emission characteristics between them.
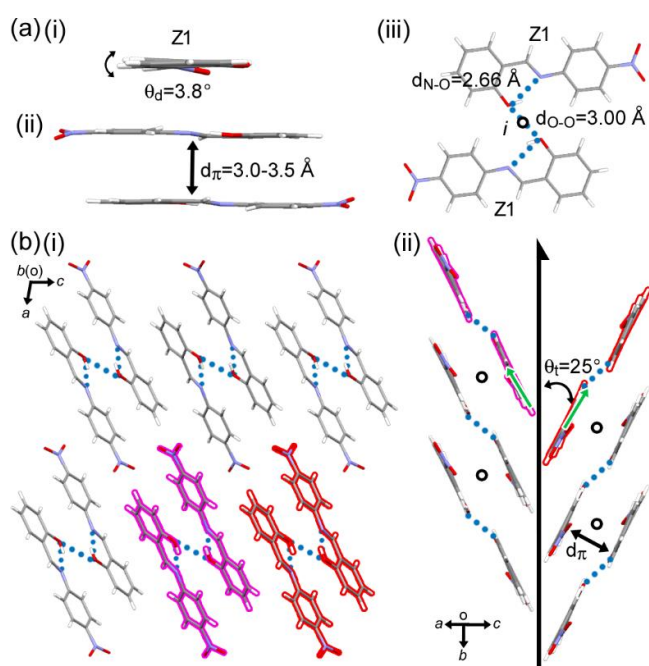
Figure 4 Crystallographic studies of 1Y. (a) (i) Dihedral angle between the two phenyl rings, (ii) distance between π-stacked molecules, (iii) hydrogen-bonding dimer, (b) (i) packing diagram, and (ii) side view of a right-handed two-fold helix by neighboring columns in **1Y**. The helical handedness is defined by tilt (green arrow) of the dimer according to the supramolecular-tilt-chirality method.[56–58]

Relative Stability of 1O and 1Y. The domino transformation from **1O** to **1Y** by mechanical stimuli suggests that **1Y** is more stable than **1O**. The relative stability was further evaluated by recourse to theoretical calculation (Table 1). Calculations were conducted on the crystal structures determined by MicroED using CONFLEX (MMFF94s) by restraining dihedral angles of the two phenyl groups (θ_d=144°(Z1)/−145°(Z2) and 176° in **1O** and **1Y**, respectively) as well as the nitro group (C-C-N-O: −4.8°(Z1)/−6.1°(Z2) and −7.8° in **1O** and **1Y**, respectively).[59,60] The calculated lattice energies of E_{1O}=−33.6 kcal mol^{-1} and E_{1Y}=−46.5 kcal mol^{-1} supported the relative stability of **1Y** over **1O**. Heating under an optical microscope showed that **1O** melts at lower temperature (ca. 120 °C) than **1Y** (ca. 160 °C), indicating that the crystal packing of **1Y** is more stable than **1O**.

Table 1 Calculated lattice energies (kcal mol^{-1}) of 1Y and 1O.

	1O	**1Y**
Lattice Energy	−33.5982	−46.4834[a]

[a] The original value is −23.2417 for Z'=1 in **1Y** and was doubled for comparison with the value of Z'=2 in **1O**.

Mechanistic studies of the domino transformation. Based on the crystallographic studies, the domino transformation from **1O** to **1Y** coupled with emission change is described by molecular conformational changes as well as molecular rearrangement in the crystal lattice. Phenyl rings rotate more than 30°, *i.e.,* from θ_d=36.2° and 35.1° in **1O** to θ_d=3.8° in **1Y**. One of the possible molecular movements is schematically shown in Fig. 5. Hydrogen-bonding

dimers in a column rotate clockwise or counterclockwise along with the conformational change. As a result, the dimers in a column and those in the neighboring column stack alternately to form **1Y**. Interestingly, electron microscope images of **1Y** crystals often had cracks in the middle and/or jagged ends, while **1O** crystals tended to be straighter (Supporting information Fig. S1). This might have resulted from internal stress caused by the transformation.
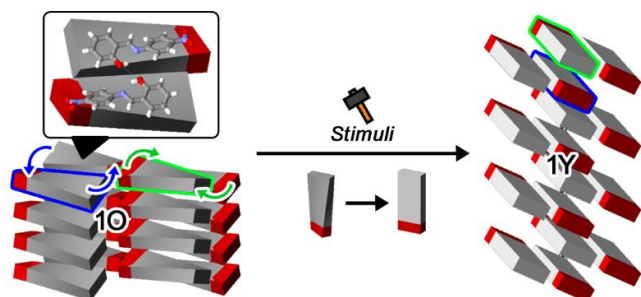
Figure 5 Transformation mechanism. Schematic representation of the molecular domino transformation mechanism from **1O** to **1Y**.

Conclusion

In conclusion, we discovered and characterized a Schiff base crystal of **1** showing mechanically-induced molecular domino transformation. Spectrometry revealed changes in emission color and intensity by the transformation (peak top shift of ca. 50 nm and over 9-fold increase of the intensity). Nanoindentation studies quantified the absolute values of the mechanical force necessary for the transformation (1 µN at the smallest). **1** is attractive as a sensing material because of the mechanical sensitivity and large emission change. Molecular domino transformation amplifies a local stimulus to a response by the whole crystal. Atomic level insights of the transformation mechanism were obtained by solving the crystal structure of a metastable **1O** by MicroED. Other series of Schiff bases, which show polymorph-dependent emission differences, are under investigation to rationally improve and control properties suitable for sensing applications based on fundamental understanding of molecular domino transformation.

ASSOCIATED CONTENT

Supporting Information. Cryo-EM images, distribution of unit cell parameters, crystallographic data, powder X-ray diffraction patterns, theoretical calculation results, and fluorescence lifetimes. This material is available free of charge via the Internet at http://pubs.acs.org. Crystal structures of **1O** and **1Y** were deposited to CCDC-2279131/COD-3000450, CCDC-2279132/COD-3000451, respectively. Results of computational chemistry were deposited to Zenodo (DOI: 10.5281/zenodo.8260131). Raw diffraction images were deposited to XRDa-142. Scripts for MicroED data collection and processing are available at https://github.com/GKLabIPR/MicroED.

AUTHOR INFORMATION

Present Address

†Japan Synchrotron Radiation Research Institute, 1-1-1 Kouto, Sayo-cho, Sayo-gun, Hyogo 679-5198, Japan

Email: toshiyuki.sasaki@spring8.or.jp

Author Contributions

The manuscript was written through contributions of all authors.

Notes
The authors declare no competing financial interest.

ACKNOWLEDGMENT

REFERENCES

(1) Bamfield, P. & Hutching, M. G. *Chromic Phenomena: Technological Applications of Colour Chemistry*, Second Edition (Royal Society of Chemistry, 2010).

(2) Kato, M., Ito, H., Hasegawa, M. & Ishii, K. Soft crystals -flexible response systems with high structural order, *Chem. Eur. J.* **25**, 5105–5112 (2019).

(3) Zheng, Y., Jia, X., Li, K., Xu, J. & Bu X.-H. Energy conversion in single-crystal-to-single-crystal phase transition materials. *Adv. Energy Mater.* 2100324 (2021).

(4) Cohen, M. D., Schmidt, G. M. J. & Flavian, S. Topochemistry. Part VI. Experiments on photochromy and thermochromy of crystalline anils of salicylaldehydes. *J. Chem. Soc.* 2041–2051 (1964).

(5) Bregman, J., Leiserowitz, L. & Schmidt, G. M. J. Topochemistry. Part IX. The crystal and molecular structures of *N*-5-chlorosalicylideneaniline near 90 and 300°K. *J. Chem. Soc.* 2068–2085 (1964).

(6) Mutai, T., Satou, H. & Araki, K. Reproducible on–off switching of solid-state luminescence by controlling molecular packing through heat-mode interconversion. *Nat. Mater.* **4**, 685–687 (2005).

(7) Mutai, T., Tomoda, H., Ohkawa, T., Yabe, Y. & Araki, K. Switching of polymorph-dependent ESIPT luminescence of an imidazo[1,2-*a*]pyridine derivative. *Angew. Chem. Int. Ed.* **47**, 9522–9524 (2008).

(8) Hino, Y., Hayashi, S. Thermotriggered domino-like single-crystal-to-single-crystal phase transition from face-to-edge to face-to-face packing of anthracenes. *Chem. Eur. J.* **27**, 17595–17600 (2021).

(9) Fukushima, M., Sato, K., Fujimoto, Y., Ito, F. & Katoh, R. Observation of an intermediate state in the solid–solid phase transition of a single crystal of perylene. *Cryst. Growth Des.* **22**, 2071–2075 (2022).

(10) Sagara, Y., Mutai, T., Yoshikawa, I. & Araki, K. Material design for piezochromic luminescence: hydrogen-bond-directed assemblies of a pyrene derivative. *J. Am. Chem. Soc.* **129**, 1520–1521 (2007).

(11) Ito, H. et al. Mechanical stimulation and solid seeding trigger single-crystal-to-single-crystal molecular domino transformations. *Nat. Commun.* **4**, 2009 (2013).

(12) Jin, M., Sumitani, T., Sato, H., Seki, T. & Ito, H. Mechanical-simulation-triggered and solvent-vapor-induced reverse single-crystal-to-single-crystal phase transitions with alterations of the luminescence color. *J. Am. Chem. Soc.* **140**, 2875–2879 (2018).

(13) Hayashi, S. & Koizumi, T. Elastic organic crystals of a fluorescent π-conjugated molecule. *Angew. Chem. Int. Ed.* **55**, 2701–2704 (2016).

(14) Mutai, T et al. A superelastochromic crystal. *Nat. Commun.* **11**, 1824 (2020).

(15) Bhattacharya, B. et al. Mechanical-bending-induced fluorescence enhancement in plastically flexible crystals of a GFP chromophore analogue. *Angew. Chem. Int. Ed.* **59**, 19878–19883 (2020).

(16) Hadjoudis, E. & Mavridis, I. M. Photochromism and thermochromism of schiff bases in the solid state: structural aspects. *Chem. Soc. Rev.* **33**, 579–588 (2004).

(17) Amimoto, K. & Kawato, T. Photochromism of organic compounds in the crystal state. *J. Photochem. Photobiol. C.* **6**, 207–226 (2005).

(18) Kobatake, S., Takami, S., Muto, H., Ishikawa, T. & Irie, M. Rapid and reversible shape changes of molecular crystals on photoirradiation. *Nature*, **446**, 778–781 (2007).

(19) Kato, M., Omura, A., Toshikawa, A., Kishi, S. & Sugimoto, Y. Vapor-induced luminescence switching in crystals of the syn isomer of a dinuclear (bipyridine)platinum(II) complex bridged with pyridine-2-thiolate ions. *Angew. Chem., Int. Ed.* **41**, 3183−3185 (2002).

(20) Ogoshi, T., Shimada, Y., Sakata, Y., Akine, S. & Yamagishi, T. A. Alkane-shape-selective vapochromic behavior based on crystal-state host–guest complexation of pillar[5]arene containing one benzoquinone unit. *J. Am. Chem. Soc.* **139**, 5664–5667 (2017).

(21) Hisaki, I. et al. Acid responsive hydrogen-bonded organic frameworks. *J. Am. Chem. Soc.* **141**, 2111–2121 (2019).

(22) Zhang, Z. et al. Two-dimensional organic single crystals with scale regulated, phase-switchable, polymorphism-dependent, and amplified spontaneous emission properties. *J. Phys. Chem. Lett.* **7**, 1697–1702 (2016).

(23) Borbone, F. et al. On−off mechano-responsive switching of ESIPT luminescence in polymorphic *N*-Salicylidene-4-amino-2-methylbenzotriazole. *Cryst. Growth Des.* **17**, 5517–5523 (2017).

(24) Varughese, S., Kiran, M. S. R. N., Ramamurty, U. & Desiraju, G. R. Nanoindentation in crystal engineering: quantifying mechanical properties of molecular crystals. *Angew. Chem. Int. Ed.* **52**, 2701–2712 (2013).

(25) Mishra, M. K., Desiraju, G. R., Ramamurty, U. & Bond, A. D. Studying microstructure in molecular crystals with nanoindentation: Intergrowth polymorphism in felodipine. *Angew. Chem. Int. Ed.* **53**, 13102–13105 (2014).

(26) Mishra, M. K., Ramamurty, U. & Desiraju, G. R. Mechanical property design of molecular solids. *Curr. Opin. Solid State Mater. Sci.* **20**, 361–370 (2016).

(27) Devarapalli, R. et al. Remarkably distinct mechanical flexibility in three structurally similar semiconducting organic crystals studied by nanoindentation and molecular dynamics. *Chem. Mater.* **31**, 1391–1402 (2019).

(28) Gruene, T. et al. Rapid structure determination of microcrystalline molecular compounds using electron diffraction. *Angew. Chem. Int. Ed.* **57**, 16313–16317 (2018).

(29) Ito, S. et al. Structure determination of small molecule compounds by an electron diffractometer for 3D ED/MicroED. *CrystEngComm* **23**, 8622–8630 (2021).

(30) Jones, C. G. et al. The cryoEM method microED as a powerful tool for small molecule structure determination. *ACS Cent. Sci.* **4**, 1587–1592 (2018).

(31) Newman, J. A. et al. From powders to single crystals: A crystallographer's toolbox for small-molecule structure determination. *Mol. Pharm.* **19**, 2133–2141 (2022).

(32) Lightowler, M. et al. Indomethacin polymorph δ revealed to be two plastically bendable crystal forms by 3D electron diffraction: Correcting a 47-year-old misunderstanding. *Angew. Chem. Int. Ed.* **61**, e202114985 (2022).

(33) Hitchen, J. et al. Organic cocrystals of TCNQ and TCNB based on an orthocetamol backbone solved by three-dimensional electron diffraction. *Cryst. Growth Des.* **22**, 1155–1163 (2022).

(34) Sasaki, T., Nakane, T., Kawamoto, A., Nishizawa, T. & Kurisu, G. Microcrystal electron diffraction (MicroED) structure determination of a mechanochemically synthesized co-crystal not affordable from solution crystallization. *CrystEngComm* 25, 352–356 (2023).

(35) Gogoi, D. et al. Structure elucidation of olanzapine molecular salts by combining mechanochemistry and micro-electron diffraction. *Cryst. Growth Des.* 2023 in press (DOI: 10.1021/acs.cgd.3c00432).

(36) Mutai, T., Shono, H., Shigemitsu, Y. & Araki, K. Three-color polymorph-dependent luminescence: Crystallographic analysis and theoretical study on excited-state intramolecular proton transfer (ESIPT) luminescence of cyano-substituted imidazo[1,2-*a*]pyridine. *CrystEngComm* **16**, 3890–3895 (2014).

(37) Konoshima, H. et al. Excited-state intramolecular proton transfer and charge transfer in 2-(2´-hydroxyphenyl)benzimidazole crystals studied by polymorphs-selected electronic spectroscopy. *Phys. Chem. Chem. Phys.* **14**, 16778–16457 (2012).

(38) Padalkar, V. S. & Seki, S. Excited-state intramolecular proton-transfer (ESIPT)-inspired solid state emitters. *Chem. Soc. Rev.* **45**, 169–202 (2016).

(39) Bond, A. D., Boese, R. & Desiraju, G. R. On the polymorphism of aspirin: Crystalline aspirin as intergrowths of two "polymorphic" domains. *Angew. Chem. Int. Ed.* **46**, 618–622 (2007).

(40) Smalley, C. J. H. et al. A structure determination protocol based on combined Analysis of 3D-ED data, powder XRD data, solid-state NMR data and DFT-D calculations reveals the structure of a new polymorph of l-tyrosine. *Chem. Sci.* **13**, 5277–5288 (2022).

(41) Lu, H. et al. B/N-doped *p*-arylenevinylene chromophores: synthesis, properties, and microcrystal electron crystallographic study. *J. Am. Chem. Soc.* **142**, 18990–18996 (2020).

(42) Hamada, H. et al. Spiro-conjugated carbon/heteroatom-bridged *p*-phenylenevinylenes: Synthesis, properties, and microcrystal electron crystallographic analysis of racemic solid solutions. *Bull. Chem. Soc. Jpn.* **93**, 776–782 (2020).

(43) Winter, G. et al. DIALS: Implementation and evaluation of a new integration package. *Acta Cryst.* **D74**, 85–97 (2018).

(44) Clabbers, M. T. B., Gruene, T., Parkhurst, J. M., Abrahams, J. P. & Waterman, D. G. Electron diffraction data processing with DIALS. *Acta Cryst.* **D74**, 506–518 (2018).

(45) Beilsten-Edmands, J. et al. Scaling diffraction data in the DIALS software package: algorithms and new approaches for multi-crystal scaling. *Acta Cryst.* **D76**, 385–399 (2020).

(46) Gildea, R. J. et al. xia2.multiplex: A multi-crystal data-analysis pipeline, *Acta Cryst.* **D78**, 752–769 (2022).

(47) Burgess, J., Fawcett, J., Russell, D. R., Gilani, S. R. & Palma, V. Four *N*-(2-hydroxybenzylidene)aniline derivatives. *Acta Cryst.* **C55**, 1707–1710 (1999).

(48) Kondori, T. et al. A novel Schiff base ligand and its copper complex: Synthesis, characterization, X-ray crystal structure and biological evaluation. *J. Mol. Struct. 1226*, 129395 (2021).

(49) Sheldrick, G. M. SHELXT - Integrated space-group and crystal-structure determination. *Acta Cryst.* **A71**, 3–8 (2015).

(50) Sheldrick, G. M. Crystal structure refinement with SHELXL. *Acta Cryst.* **C71**, 3–8 (2015).

(51) Dolomanov, O. V., Bourhis, L. J., Gildea, R. J., Howard, J. A. K. & Puschmann, H. OLEX2: A complete structure solution, refinement and analysis program. *J. Appl. Cryst.* **42**, 339–341 (2009).

(52) Bourhis, L. J., Dolomanov, O. V., Gildea, R. J., Howard, J. A. K., Puschmann, H. *Acta Cryst.* **A71**, 59–75 (2015).

(53) Knyazhansky, M. I., Metelitsa, A. V., Bushkov, A. J. & Aldoshin, S. M. Role of structural flexibility in fluorescence and photochromism of the salicylideneaniline: The "aldehyde" ring rotation. *J. Photochem. Photobiol. A* **97**, 121–126 (1996).

(54) Grabowski, Z. R., Rotkiewicz, K. & Rettig, W. Structural changes accompanying intramolecular electron transfer: Focus on twisted intramolecular charge-transfer states and structures. *Chem. Rev.* **103**, 3899–4032 (2003).

(55) Sasaki, S., Drummen, G. P. C. & Konishi, G.-I. Recent advances in twisted intramolecular charge transfer (TICT) fluorescence and related phenomena in materials chemistry. *J. Mater. Chem. C* **4**, 2731–2743 (2016).

(56) Hisaki, I., Sasaki, T., Tohnai, N. & Miyata, M. Supramolecular-tilt-chirality on two-fold helical assemblies. *Chem. Eur. J.* **18**, 10066–10073 (2012).

(57) Sasaki, T. et al. Linkage control between molecular and supramolecular chirality in 2_1-helical hydrogen-bonded networks using achiral components. *Nat. Commun.* **4**, 1787 (2013).

(58) Miyata, M., Tohnai, N., Hisaki, I. & Sasaki, T. Generation of supramolecular chirality around twofold rotational or helical axes in crystalline assemblies of achiral components. *Symmetry* **7**, 1914–1928 (2015).

(59) Goto, H., Obata, S., Nakayama, N. & Ohta, K. *CONFLEX 8*, CONFLEX Corporation, Tokyo, Japan, 2017.

(60) Halgren, T. A. Merck molecular force field. I. Basis, form, scope, parameterization, and performance of MMFF94. *J. Comput. Chem.* **17**, 490–519 (1996).

Supplementary Information

Mechanically-Sensitive Fluorochromism by Molecular Domino Transformation in a Schiff Base Crystal

Toshiyuki Sasaki,[a]*† Takanori Nakane,[b] Akihiro Kawamoto,[b] Yakai Zhao,[c,d] Yushi Fujimoto,[e] Tomohiro Nishizawa,[f] Fuyuki Ito,[d]* Upadrasta Ramamurty,[c,d]* Ranjit Thakuria,[g]* Genji Kurisu[b,h,i]*

Affiliation

[a]*Graduate School of Nanobioscience, Yokohama City University; 22-2 Seto; Kanazawa-ku, Yokohama, Kanagawa 236-0027, Japan. E-mail: tsasaki@yokohama-cu.ac.jp*

[b]*Institute for Protein Research, Osaka University, 3-2 Yamadaoka, Suita, Osaka 565-0871, Japan.*

[c]*School of Mechanical and Aerospace Engineering, Nanyang Technological University, Singapore 639798, Singapore. Email: satwiku@gmail.com*

[d]*Institute of Materials Research and Engineering, Agency for Science, Technology and Research (A*STAR), Singapore 138634, Singapore.*

[e]*Department of Chemistry, Institute of Education, Shinshu University, 6-ro, Nishinagano, Nagano, 380-8544, Japan. Email: fito@shinshu-u.ac.jp*

[f]*Graduate School of Medical Life Science, Yokohama City University, 1-7-29 Suehiro-cho, Tsurumi-ku, Yokohama 230-0045, Japan.*

[g]*Department of Chemistry, Gauhati University, Guwahati 781014, Assam, India. Email: ranjit.thakuria@gmail.com, ranjit.thakuria@gauhati.ac.in*

[h]*JEOL YOKOGUSHI Research Alliance Laboratories, Graduate School of Frontier Biosciences, Osaka University, 1-3 Yamadaoka, Suita, Osaka 565-0871 Japan.*

[i]*Institute for Open and Transdisciplinary Research Initiatives, Osaka University, 2-1 Yamadaoka, Suita, Osaka 565-0871, Japan. Email: gkurisu@protein.osaka-u.ac.jp*

†Present address: *Japan Synchrotron Radiation Research Institute (JASRI), Kouto, Sayo-cho, Sayo-gun, Hyogo 679-5198, Japan. Email: toshiyuki.sasaki@spring8.or.jp*
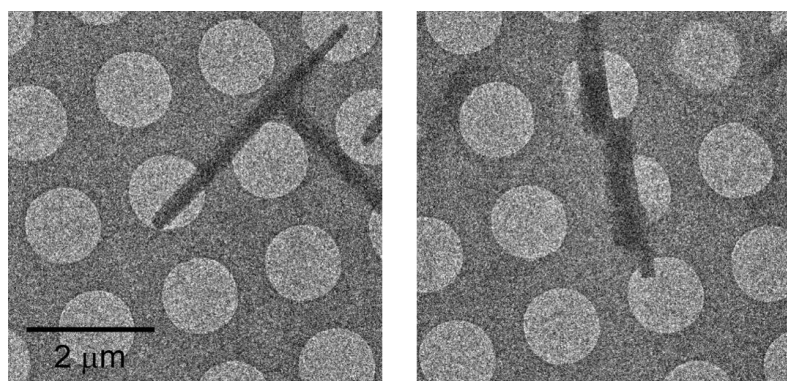
Figure S1 Typical Cryo-EM images of 1. The crystal in the left panel was indexed in the orthorhombic crystal system (**1O**), while the crystal in the right panel was indexed in the monoclinic crystal system (**1Y**). Images of other crystals are deposited in XRDa.
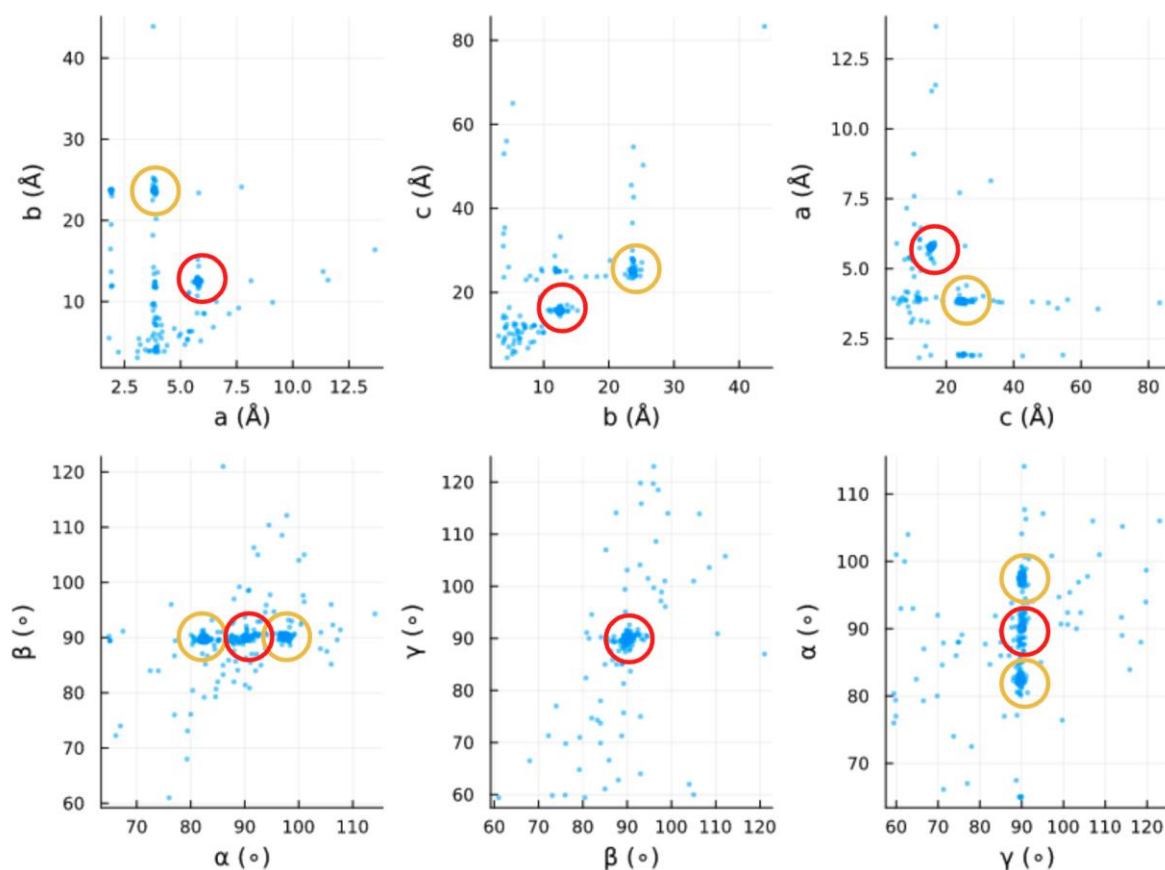
Figure S2 Distribution of unit cell parameters from the first indexing trial. Note that Bravais lattice constraints were not applied and the diffraction geometry was not fully refined at this initial step of processing. Some dots correspond to mis-indexed, very weakly diffracting crystals. Monoclinic (**1Y**) and orthorhombic (**1O**) crystal forms are present and marked by orange and red circles, respectively. Monoclinic crystals are indexed in two settings (the *β* angle is split symmetrically around 90° to ~82° and ~98°).

Table S1 Merging statistics of 1O by MicroED.

d_max	d_min	#obs	#uniq	mult.	%comp	<I>	<I/sI>	r_mrg	r_means	r_pim	cc1/2
5.86	2.01	1050	164	6.40	84.54	2.9	20.1	0.089	0.096	0.034	0.996*
2.01	1.61	1901	196	9.7	100.00	1.4	12.5	0.164	0.172	0.048	0.996*
1.61	1.41	1469	170	8.64	100.00	0.6	5.1	0.235	0.248	0.076	0.983*
1.41	1.28	1154	151	7.64	100.00	0.4	3.0	0.289	0.308	0.100	0.970*
1.28	1.19	1909	181	10.55	100.00	0.5	3.6	0.269	0.282	0.080	0.995*
1.19	1.12	1814	177	10.25	100.00	0.5	4.1	0.237	0.248	0.069	0.991*
1.12	1.06	1673	164	10.2	100.00	0.3	2.7	0.334	0.349	0.096	0.976*
1.06	1.02	1466	156	9.4	100.00	0.3	2.3	0.32	0.337	0.099	0.974*
1.02	0.98	1365	150	9.1	100.00	0.2	1.3	0.504	0.533	0.162	0.936*
0.98	0.94	1416	153	9.25	100.00	0.2	1.0	0.553	0.582	0.170	0.919*
0.94	0.92	1975	177	11.16	100.00	0.1	0.6	0.982	1.022	0.271	0.636*
0.92	0.89	1842	166	11.1	100.00	0.1	0.8	0.894	0.933	0.253	0.737*
0.89	0.87	1691	165	10.25	100.00	0.1	0.6	0.972	1.013	0.271	0.491*
0.87	0.84	1685	162	10.4	100.00	0.0	0.5	1.324	1.381	0.372	0.470*
0.84	0.83	1659	158	10.5	100.00	0.0	0.4	1.513	1.576	0.419	0.385*
0.83	0.81	1592	152	10.47	100.00	0.0	0.4	1.987	2.069	0.553	0.157
0.81	0.79	1327	141	9.41	100.00	0.0	0.3	2.225	2.327	0.648	0.444*
0.79	0.78	1464	147	9.96	100.00	0.0	0.4	2.35	2.450	0.661	0.608*
0.78	0.76	1355	138	9.82	100.00	0.0	0.3	2.155	2.250	0.621	0.323*
0.76	0.75	1998	182	10.98	100.00	0.0	0.2	3.637	3.787	1.001	0.280*
5.86	0.75	31805	3250	9.79	99.72	0.4	3.2	0.296	0.311	0.089	0.995*

Table S2 Merging statistics of 1Y by MicroED.

| d_max	d_min	#obs	#uniq	mult.	%comp	<I>	<I/sI>	r_mrg	r_means	r_pim	cc1/2
5.73	1.62	18417	312	59.03	96.89	8.3	38.0	0.151	0.152	0.020	0.996*
1.62	1.29	20831	289	72.08	98.30	3.0	24.9	0.198	0.199	0.022	0.990*
1.29	1.13	19005	278	68.36	98.58	3.0	20.9	0.199	0.201	0.024	0.990*
1.13	1.02	23324	292	79.88	98.32	2.5	21.0	0.21	0.212	0.023	0.966*
1.02	0.95	19247	270	71.29	98.54	1.2	10.9	0.318	0.320	0.036	0.993*
0.95	0.90	23405	295	79.34	98.33	1.0	9.8	0.339	0.341	0.037	0.970*
0.90	0.85	20491	270	75.89	98.18	0.7	7.2	0.439	0.442	0.049	0.964*
0.85	0.81	20343	273	74.52	98.56	0.5	5.0	0.562	0.567	0.064	0.889*
0.81	0.78	24240	288	84.17	98.63	0.5	5.3	0.529	0.532	0.056	0.982*
0.78	0.76	20951	275	76.19	97.86	0.3	3.5	0.72	0.726	0.080	0.879*
0.76	0.73	20493	266	77.04	98.15	0.3	3.0	0.777	0.783	0.086	0.849*
0.73	0.71	21569	280	77.03	98.94	0.2	2.3	0.918	0.925	0.103	0.810*
0.71	0.69	23230	280	82.96	98.25	0.2	2.4	0.921	0.927	0.099	0.805*
0.69	0.68	22843	280	81.58	98.94	0.2	2.0	1.12	1.128	0.122	0.823*
0.68	0.66	20625	262	78.72	98.50	0.2	1.8	1.291	1.300	0.141	0.834*
0.66	0.65	20223	273	74.08	98.56	0.1	1.1	1.67	1.683	0.190	0.603*
0.65	0.63	22338	284	78.65	98.95	0.1	1.1	1.777	1.790	0.195	0.800*
0.63	0.62	21517	258	83.40	98.47	0.1	0.9	2.174	2.190	0.234	0.260*
0.62	0.61	23945	289	82.85	98.97	0.1	0.9	2.262	2.278	0.242	0.326*
0.61	0.60	21309	266	80.11	98.52	0.1	0.7	2.794	2.814	0.302	0.244*
5.73	0.6	428346	5580	76.76	98.41	1.2	8.4	0.327	0.330	0.037	0.995*
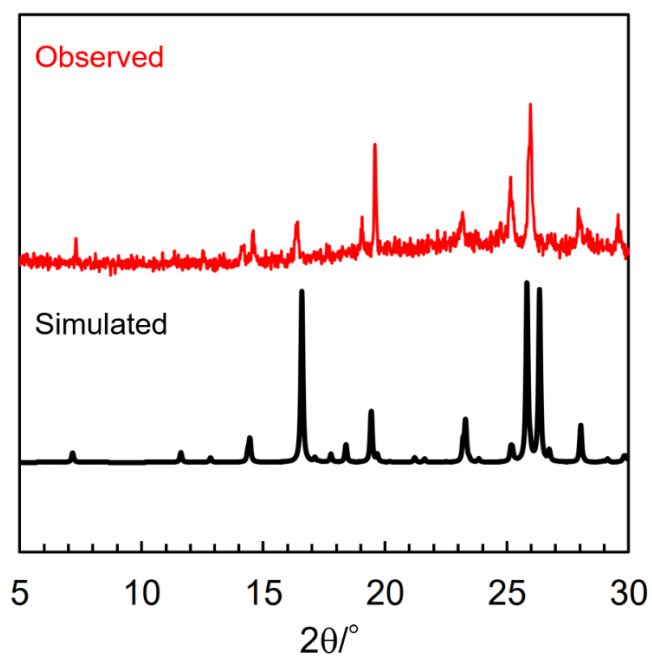
Figure S3 Powder X-ray diffraction patterns of 1Y. One is measured at room temperature (Observed, red solid line) and the other is simulated from the crystal structure solved by MicroED (black solid line).

Table S3 Crystallographic parameters of 1O and 1Y solved by MicroED (λ = 0.02508 Å).

Polymorphs	**1O**	**1Y**
Chemical formula	C13 H10 N2 O3	C13 H10 N2 O3
Formula wt	242.23	242.23
Cryst syst	Orthorhombic	Monoclinic
Space group	$Pna2_1$	$P2_1/c$
T, K	79	79
a, Å	23.456	12.450
b, Å	3.811	5.735
c, Å	24.879	15.344
α, deg	90	90
β, deg	90	97.73
γ, deg	90	90
Z	8	4
V, Å^3	2224.2	1085.6
D_{calc}, g cm^{-3}	1.447	1.482
reflns collected	21049	208643
unique reflns	3836	2657
R1[I > 2(I)]	0.1215	0.1774
wR2 (all)	0.3097	0.4522
GOF	0.864	1.253
Data collection	Talos Arctica microscope	Talos Arctica microscope
High resolution limit for refinement, Å	0.84	0.75
COD ID.	3000450	3000451
CCDC no.	2279131	2279132

Table S4 Crystallographic parameters of 1O and 1Y optimized by CONFLEX (MMFF94s).

Polymorphs	1O	1Y
a /Å	23.4560	12.4500
b /Å	3.8110	5.7350
c /Å	24.8790	15.3440
α /deg	90	90
β /deg	90	97.7300
γ /deg	90	90
V /Å^3	2223.9541	1085.6175
D / g cm^{-3}	1.4459	1.4811
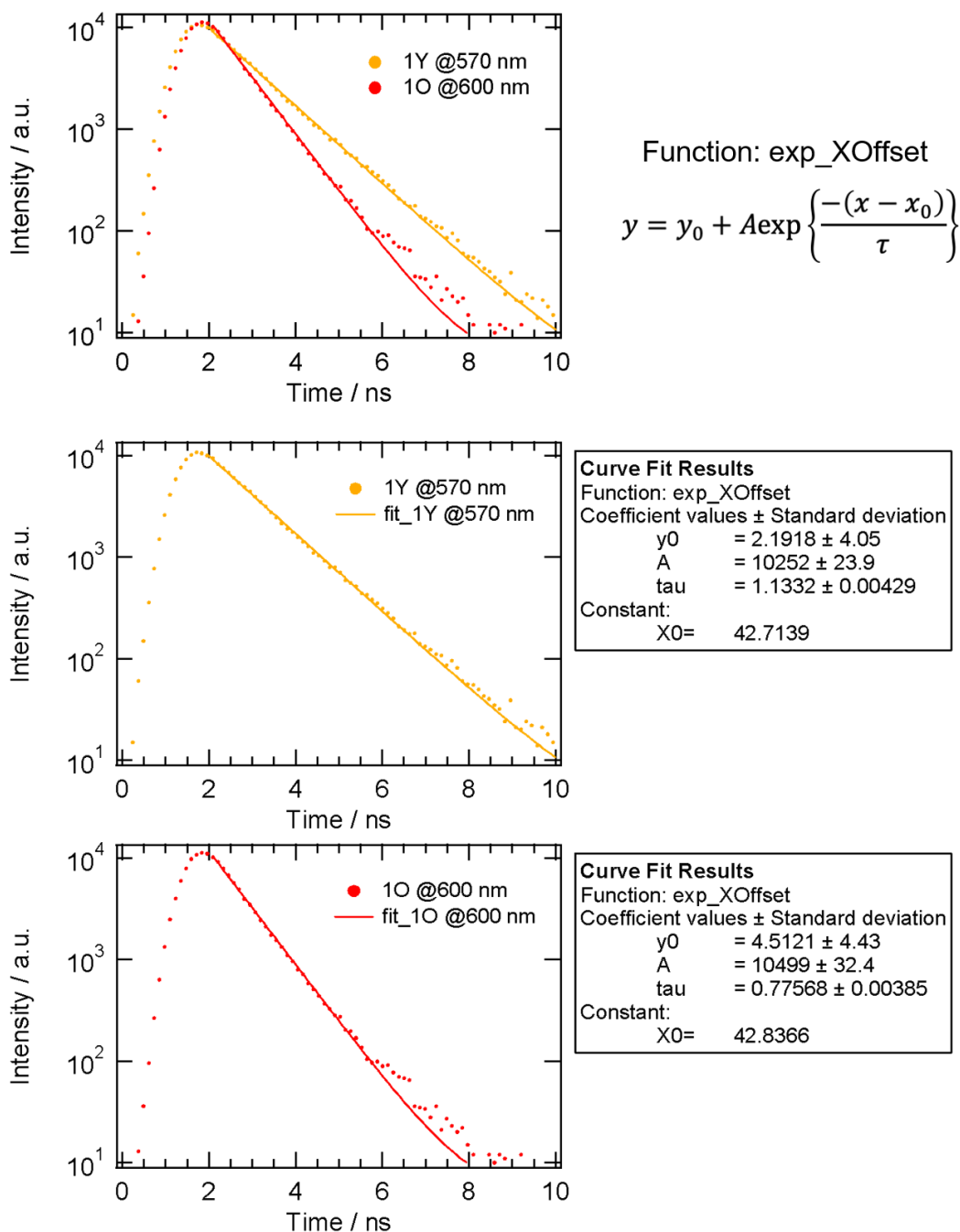
Figure S4 Fluorescence lifetimes of 1Y and 1O. The lifetimes were measured by a unit consisted of a pico pulse laser (375 nm, 50 MHz) (LDB 160C, Tama Electric Inc.), an avalanche photodiode detector (MPD, Becker & Hickl GmbH), and a counting board (SPC-130, Becker & Hickl GmbH). Filters: a sharp-cut filter (L42, HOYA), and optical bandpass filters (570 nm or 600 nm, 10 nm bandwidth in fwhm), were used to select the monitoring wavelength and avoid the scattering excitation light.